American Journal of
Botany

Ontogenetic scaling of phloem sieve tube anatomy and hydraulic resistance with tree height in *Quercus rubra*

Laura E. Clerx[1] , Fulton E. Rockwell[1] , Jessica A. Savage[2] , and N. Michele Holbrook[1,3]

PREMISE: The dimensions of phloem sieve elements have been shown to vary as a function of tree height, decreasing hydraulic resistance as the transport pathway lengthens. However, little is known about ontogenetic patterns of sieve element scaling. Here we examine within a single species (*Quercus rubra*) how decreases in hydraulic resistance with distance from the plant apex are mediated by overall plant size.

METHODS: We sampled and imaged phloem tissue at multiple heights along the main stem and in the live crown of four size classes of trees using fluorescence and scanning electron microscopy. Sieve element length and radius, the number of sieve areas per compound plate, pore number, and pore radius were used to calculate total hydraulic resistance at each sampling location.

RESULTS: Sieve element length varied with tree size, while sieve element radius, sieve pore radius, and the number of sieve areas per compound plate varied with sampling position. When data from all size classes were aggregated, all four variables followed a power-law trend with distance from the top of the tree. The net effect of these ontogenetic scalings was to make total hydraulic sieve tube resistance independent of tree height from 0.5 to over 20 m.

CONCLUSIONS: Sieve element development responded to two pieces of information, tree size and distance from the apex, in a manner that conserved total sieve tube resistance across size classes. A further differentiated response between the phloem in the live crown and in the main stem is also suggested.

KEY WORDS   allometry; Fagaceae; long distance transport; phloem anatomy; plant vascular architecture; plant vascular transport.

The idea that photosynthates are transported through the phloem via an osmotically generated gradient in turgor pressure was first proposed by Ernst Münch (Münch, 1930; Knoblauch and Peters, 2010). According to this mechanism, the source of the pressure gradient is the influx of water by osmosis when sugars are loaded in phloem source tissue and the corresponding efflux of waters as sugars are utilized for growth and respiration by sink tissues (Thompson and Holbrook, 2003; Jensen et al., 2016). Although this explanation has been accepted as adequate to account for the transport of photosynthate through small plants, whether it is sufficient to explain phloem transport in tall trees has long been questioned (e.g., Canny, 1973; Lang, 1979; c.f. Taiz et al., 2015). At issue has been whether the hydraulic resistance to flow in large/long plants is too great to allow osmotic pressures generated in the leaves to drive the flow of photoassimilates all the way to the roots (Tyree et al., 1974; Thompson, 2006; Turgeon, 2010).

Recent work pointing to anatomical changes in the phloem as plants increase in size provides a strong basis for asserting the sufficiency of Münch flow to explain phloem transport in tall trees and long vines (Petit and Crivellaro, 2014; Knoblauch et al., 2016; Liesche et al., 2017; Savage et al., 2017). These results suggest that structural modification of a plant's carbohydrate transport infrastructure solves the "problem" of organismal size and stature by reducing phloem hydraulic resistance. Compensating anatomical changes with height are consistent with cambial responses to positional information such as may be derived from auxin gradients, responses known to drive variation in xylem characteristics in different tissues and growth stages (Dengler, 2001; Aloni, 2015). Indeed, Petit and Crivellaro (2014) showed that, in three young trees of different species (*Picea abies*, *Fraxinus excelsior*, *Salix eleagnos*), both xylem and phloem conduit diameters widen over 10 sampling positions

from plant apex to base. Savage et al. (2017) reported a similar pattern for phloem anatomy in mature trees of 10 angiosperm species, finding also that xylem vessel resistivity scaled with sieve tube resistivity. Both of these studies fit anatomical data such as sieve element diameter and length to "distance from the top" of a tree by imposing a power-law relationship, a form motivated by metabolic scaling arguments (e.g., West et al., 1999) and which, in this context, describes a *rate* of change with height that is large near the top and lessens toward the base. A power-law relationship as a function of stem length was also fit by Olson et al. (2014) to the mean hydraulic diameter of vessels near the base of 257 angiosperms. Yet, organ age may affect these patterns. Mäkelä et al. (2019) showed that, in current year shoots of two conifers, tracheid diameter scaled with the local under bark shoot diameter and the *relative* (not absolute) distance from the shoot apex.

For hierarchical branching networks such as the xylem and phloem, theoretical expectations for "optimal" scalings between measures of plant size (total mass or height) and conduit dimensions have been generated by minimizing hydrodynamic resistance (West et al., 1999) or hydrodynamic resistance plus a constraint based on a volumetric cost function for the sap, as inspired by models of blood flow (Murray 1926; McCulloh et al., 2003; see Williams et al. (2019) for a recent discussion of this literature). As discussed by Sevanto (2014), these approaches treat flow as purely axial (i.e., Hagen–Poiseuille flow), whereas phloem (and xylem) conduits are permeable on the radial walls, and therefore we should expect a radial component to the flow to the extent conduits gain or lose water from the surrounding tissues. Modelling of such "leaky pipe" flow shows that as water "leaks" in or out radially, the flow accelerates or decelerates, and the pressure gradient diverges from the linear drop expected for purely axial flow (Phillips and Dungan, 1993; Knoblauch and Peters, 2010; Jensen et al., 2012b). In the phloem, there is a further layer of complexity due to osmotic effects: as the phloem sap travels out of the sugar-loading zone into the translocation zone, viscous dissipation of the pressure (as well as increases in the water potential of surrounding tissue, as might occur for phloem transport against transpiration induced water potential gradients) drive water into the phloem, further increasing the volume flow rate while diluting the osmotic potential of the sap (Phillips and Dungan, 1993; Jensen et al., 2012b). As a result, scaling relations based on optimization of viscous losses for purely axial flow may not apply (Sevanto, 2014) or may vary between source/sink regions with radial fluxes of both sugar and water and translocation regions with a potential radial flux of water only (Jensen et al., 2012b).

Hand in hand with this theoretical uncertainty is a diversity of empirical results. As noted above, some studies find a power-law relationship between sieve element radius and distance from the treetop (Petit and Crivellaro, 2014; Savage the al., 2017). Leische et al. (2017) assembled a data set of phloem anatomical characteristics near the base of 447 angiosperm species through both new sampling and a literature search, fitting linear relationships between sieve element length, radius, sieve number, sieve pore number, sieve pore radius, and total stem length with varying degrees of success. Losada and Holbrook (2019) showed that the relationship between sieve element length, sieve element radius, and stem diameter appeared to increase geometrically with distance from the apex in the woody shrub *Illicium parviflora.* As noted by Petit and Crivellaro (2014), however, a finding of different types of allometric scaling across species does not preclude the possibility of a general power-law relationship between distance from the plant apex and phloem structure within individuals. Yet, no study to date we are aware of has examined phloem anatomy as a function of distance from the apex across different individuals and size classes within a single species.

Here we focused on *Quercus rubra* L. (Fagaceae) to determine how the anatomy of the phloem varies along the length of the plant and with different ontogenetic stages (as represented by size classes). We sought to answer the questions: As a tree grows taller, at what point in its ontogeny, or at what distance from the apical meristem, do we observe changes in the anatomy of its sieve elements that affect hydraulic resistance? If the structural proportions of sieve elements vary with distance from the plant apex, is the relationship between anatomy and distance conserved across conspecifics of different size classes? And, if observed, are changes in local phloem anatomy along the length of the tree sufficiently large that the total resistance of a hypothetical sieve tube running from plant apex to base is independent of tree height?

MATERIALS AND METHODS

Experimental design

We sampled 12 *Q. rubra* trees of four size classes, three trees per size class, at the Harvard Forest in Petersham, Massachusetts, United States. All of the trees sampled were located along the edge of the same forest clearing and therefore experienced similar exposure to sunlight, elevation, soil type, and other environmental conditions. The smallest trees had a mean height of 52.3 cm and were sampled only at their midpoint (mean sampling height 26.2 cm). We sampled the next size class (mean height 1.9 m) at the base and the top of the trees at mean sampling heights 0.13 m and 1.61 m, respectively. For the third tree size class (mean height 7 m), we sampled at the base of the stem, the midpoint of the tree, and the top of the tree, with mean sampling heights of 0.5 m, 3.4 m, and 6.3 m. For all of these trees, the base and midpoint sampling locations were along the main stem, which we consider a translocation region if transport to the roots dominates over radial stem carbohydrate storage, while the topmost sampling location was on the largest diameter vertical stem in the live crown, proximal to source regions in the leaves. For the fourth and largest tree size class (trees of mean height 21.2 m), we chose five sampling locations along the length of the tree, ranging from the base of the trunk to the top of the tree, with mean sampling heights of 0.6 m, 5.8 m, 10.2 m, 14.4 m, and 18.2 m. The base and first two midpoint sampling locations were along the main stem, the next sampling location was near the juncture between the main stem and the live crown (in some cases in the crown), and the topmost sampling location was on what we estimated to be the largest diameter vertical stem in the live crown. Each "sampling height" is the measured distance from the ground. We will refer to the individual size classes by the nominal heights of 0.5 m, 2 m, 7 m, and 21 m.

Sampling

We used wood chisels and a hammer to remove bark from the trees at each sampling locations (Fig. 1). We found that *Q. rubra* bark breaks at the vascular cambium when chiseled, with the phloem comprising the innermost layer of our sample. Access to the middle and topmost sampling locations in the trees of the two larger size classes was provided by a 22-m boom lift. We measured the height and circumference at each sampling location, then excised two, approximately 2.5 × 5 cm,
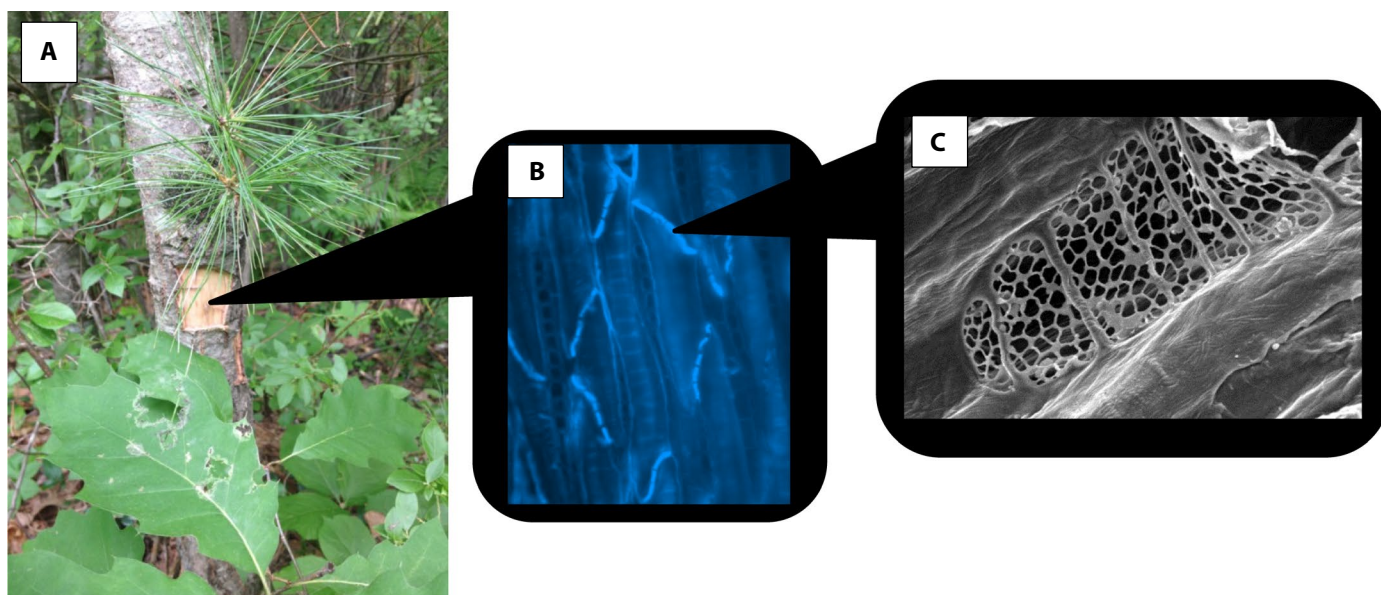
FIGURE 1. Study design. (A) Sampling location at the base of the stem of a mid-size class tree. Each phloem sample was preserved and imaged using (B) fluorescence microscopy to obtain measurements of plate angle, sieve element lumen length, sieve element radius, and the number of sieve areas per compound plate and (C) scanning electron microscopy to measure sieve plate pore radius, sieve pore area, and pore density per plate.

samples of phloem tissue. For trees of the two smaller size classes, we used large pruning shears to sever the trees at the base and then immediately sampled the phloem tissue using a single-edged razor blade to split the bark at the vascular cambium and remove the phloem tissue. This tissue was similarly divided into two samples per sampling location: one destined for fluorescence microscopy (estimation of sieve element length and radius) and the other for scanning electron microscopy (estimation of sieve plate characteristics).

Sample preparation

The samples that would be imaged via scanning electron microscopy were wrapped in aluminum foil and immediately plunged into liquid nitrogen (−196°C) to minimize callose deposition (Mullendore et al., 2010). The frozen samples were transferred to a cooler of dry ice (−78.5°C) for transportation, then stored at −80°C (Mullendore et al., 2010). We placed the samples that would be imaged with fluorescent microscopy in 45 mL plastic Falcon centrifuge tubes for approximately 10–15 min to allow the deposition of callose [ß-(1-3)-glucans] on the sieve plates (Esau and Cheadle, 1961; Mullendore et al., 2010; Knoblauch et al., 2016; Savage et al., 2017) before fixing these samples in 70% v/v ethanol.

Fluorescence microscopy

We used fluorescence imaging to determine the dimensions of the sieve elements. Using double-edged razor blades to tangentially section the innermost tissue layer, we cut sections approximately 100 µm thick. We then rinsed these sections with DI water and stained them with a 0.1% w/v aniline blue aqueous solution (excitation 370 nm, emission 509 nm) to target callose and thereby locate the sieve plates that identify a phloem cell as a sieve tube element (Savage et al., 2017). We imaged the phloem using a Leica DMI 3000B inverted microscope (Leica Microsystems, Wetzler, Germany), with a Leica A4 filter cube (excitation filter: BP 360/40, suppression filter: BP 470/40) and the

Leica LAS V4.1 imaging software program to capture approximately 50–100 images per sampling location, >2000 images in total.

Scanning electron microscopy (SEM)

We took SEM images of sieve plates using the high vacuum mode of a Jeol 6010LV scanning electron microscope (Jeol USA, Peabody, MA, USA). To prepare the phloem tissue for SEM imaging, we used single- and double-edged razor blades to make oblique sections at a variety of orientations to account for the angled nature of the sieve plates. To obtain clear SEM images, we first digested the cell contents using a solution of 0.1% w/v proteinase K in 50 mM Tris-HCL buffer, with 1.5 mM calcium acetate and 8% v/v Triton X-100. NaOH was used to adjust the pH of the solution to 8. We incubated each sample in 1.5 mL of the proteinase K digest solution in a thermomixer at 55°C for 2–3 weeks, periodically inverting them to prevent the Triton X-100 from settling out of the solution (Mullendore et al., 2010). Upon removal from incubation, we rinsed the samples in DI water, allowing them to soak for 1 h. We then used a soft tissue to absorb excess moisture before freeze-drying the samples. The freeze-dried samples were mounted on SEM pin stubs covered in carbon adhesive tape and sputter-coated with 10 nm of gold/palladium (Au/Pd) metal coating to enhance the secondary electron signal in the SEM (Arnold Arboretum, Boston, MA, USA). We took 20–30 images of sieve plates per sample, for a total of >660 SEM images captured with Jeol Technics InTouchScope1.09 software.

Image analysis

We selected fluorescence images for analysis with Image J (National Institutes of Health, Bethesda, MD, USA) based on clarity and visibility of entire sieve elements. Sieve element length was measured from the midpoint of the top sieve plate to the midpoint of the bottom sieve plate for 10 sieve elements per sampling location. We measured sieve element diameter at the midpoint of each sieve

element and the angle of one sieve plate with respect to the long axis of the sieve element for $n = 10$ sieve elements per sampling location. We also recorded the number of sieve areas because red oak has compound plates (multiple sieve areas within one plate).

We used SEM to examine the structure of the sieve plates. To avoid selection bias, a random number generator was used to choose the sieve areas to analyze from among those visible in each micrograph. We measured the major a and minor b diameters of 10 sieve areas, sampled from at least six compound plates per sampling location. Then, we assumed an elliptical sieve area shape and defined the calculated sieve area as πab. Due to the difficulty in obtaining entirely unobstructed images of entire sieve areas, we measured pore density (number per area) from the visible fraction of a given sieve area (i.e., the observed sieve area), and then estimated the adjusted pore number per sieve area as the observed pore density times the calculated total sieve area. The adjusted pore number was then multiplied by the mean number of sieve areas per compound

plate (obtained from fluorescent micrographs) to estimate the total pore number per sieve plate. Sieve plate pore areas from six plates per sample were measured for $n \geq 100$ pores per sample; from these measurements, we calculated sieve plate pore radius as the radius of the circle with area equal to the observed pore area.

Hydraulic resistance

We used our measurements of sieve element geometry to model sieve tube hydraulic resistance (Fig. 2). We consider the resistance of individual sieve tubes, rather than that of the total phloem at a given location along the stem, due to the difficulty in accurately estimating the total number of sieve tubes in the phloem tissue (Canny, 1973). For this reason, we report mean sieve element radii, rather than hydrodynamic radii, as is often reported to describe the mean effective radius of a population of xylem elements in a cross section. Following Knoblauch et al. (2016) and Savage
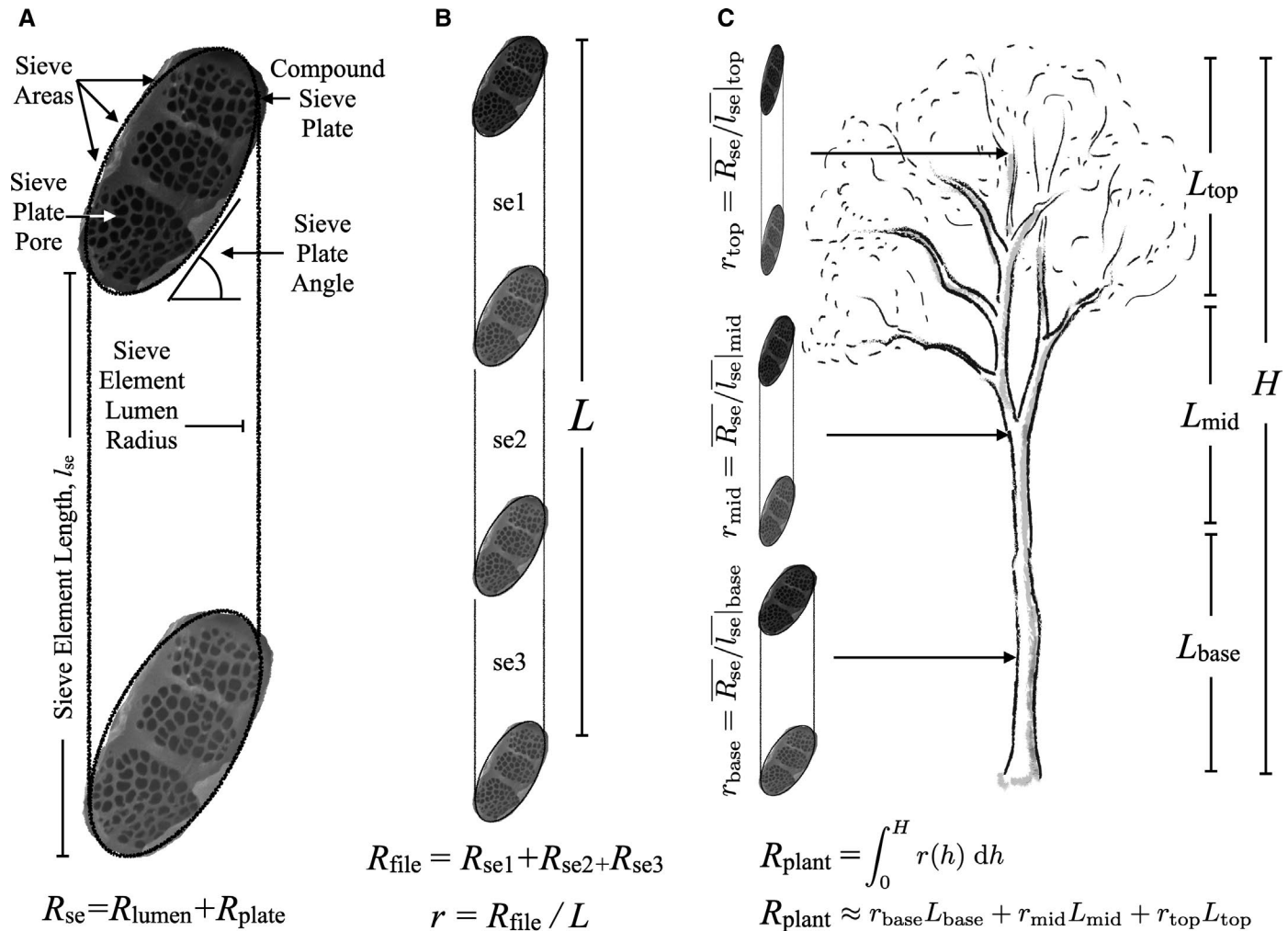

FIGURE 2. Components of sieve element, sieve tube, and "whole-plant" resistance. (A) The resistance of a single sieve element (R_{se}) is composed of a plate resistance that depends on the number and radii of the pores in a sieve area and the number of sieve areas in a compound sieve plate (effectively accounting for plate angle), in series with a lumen resistance that depends on its radius and length. (B) The resistivity (r) of a file of sieve tube elements can be defined as the sum of the resistances of the individual sieve tube elements (R_{file}) divided by their total length (L). (C) The resistance of a file of sieve tube elements (R_{plant}) spanning the height H of a tree is defined by integrating the resistivity r as a function of height h from the base ($h = 0$) to the top of the tree ($h = H$); alternatively, R_{plant} can be estimated by summing the product of the average sieve element resistivity at each sampling position and L, the length of the tree apportioned to each sampling position, from the base to the top of the tree.

et al. (2017), we used the Hagen–Poiseuille equation to describe flow through a series of sieve elements in much the same way it would be used to describe pressure-driven flow through a series of cylindrical pipes. We used the Hagen–Poiseuille model despite its failure to fully characterize osmotic flows in leaky pipes for three reasons. First, a leaky pipe model of conductance is sensitive to both the radial permeability and the choice of boundary condition for local water potential outside the radial wall, and the appropriate values cannot be obtained from anatomical observation (Jensen et al., 2012; Sevanto, 2014). Second, even in the case of leaky pipe flow, Hagen–Poiseuille locally describes the radial distributions of axial velocities, and so viscous losses, correctly (Phillips and Dungan, 1993). Given the aspect ratio of phloem conduits as long and narrow, viscous losses are expected to be important with respect to osmotic effects (i.e., inward radial fluxes of water) in determining the behavior of axial transport (Münch number <<1, Jensen et al., 2012b). Finally, in the translocation region radial permeability may be minimized by selection, as while a radial influx of water increases axial velocity, dilution of the sap means that the sugar transport rate (i.e., sap velocity times concentration) is essentially unchanged. In the translocation region, high radial permeability would then appear to result in largely futile water cycling between xylem and phloem.

With ΔP as the turgor pressure differential, η as the sap viscosity, L as the length of the sieve tube transport pathway, Q as the volumetric flow rate, and r as the radius of the sieve element lumen, we then have for Hagen–Poiseuille flow:

$$\Delta P = \frac{8\eta L Q}{\pi r^4}. \tag{1}$$

As hydraulic resistance is equal to ΔP, the driving force due to a pressure gradient, divided by Q, the volumetric flow rate, the equation for hydraulic resistance is given in its simplest form by,

$$R = \frac{8\eta L}{\pi r^4}, \tag{2}$$

where we assumed a sap viscosity η of 1.7 mPa s (16% w/w sucrose solution at 20°C, Jensen et al., 2013). Our model considers two main sources of resistance to flow through a sieve element: the sieve element lumen and the sieve plates. We define the total resistance, R_{se}, as the sum of the resistance due to the lumen and the resistance due to the sieve plate:

$$R_{se} = R_{lumen} + R_{plate}. \tag{3}$$

Using the formula for resistance derived from the Hagen–Poiseuille relationship, the hydraulic resistance through the sieve tube element lumen is given by,

$$R = \frac{8\eta L_{se}}{\pi r_{se}^4}, \tag{4}$$

such that a longer lumen length (L_{se}) increases hydraulic resistance, while a wider sieve element (r_{se}) decreases the resistance to flow.

The hydraulic resistance of the sieve plate is calculated by summing in parallel the resistance of each individual pore on the sieve plate,

$$R_p = \left(\sum R_{p,i}^{-1} \right)^{-1}, \tag{5}$$

where $R_{p,i}$ is the resistance of the ith pore. Similar to the resistance of the lumen, the calculation of hydraulic resistance due to flow through an individual pore is derived from the Hagen–Poiseuille relationship, where we assume that the thickness of the plate, and thus the length of the pore lumen, is a distance of 1 μm (Jensen et al., 2012a). The additional term, known as the Sampson correction, accounts for the entrance and exit of sieve sap from the wider sieve element lumen into the much smaller sieve plate pores:

$$R_{p,i} = \frac{8\eta l_{p,i}}{\pi r_{p,i}^4} + \frac{3\eta}{r_{p,i}^3} \tag{6}$$

Due to the difficulty of obtaining images in which all of the pores of the large compound sieve plates of Q. rubra can be measured, we used the model developed by Jensen et al. (2012) that relates the resistance of sieve plates to the mean and standard deviation of the sieve plate pore radii:

$$R_p = \frac{3\eta}{r_p^3} \frac{1}{N} \left[\frac{1}{1+3\beta^2} + \frac{\alpha}{1+6\beta^2+3\beta^4} \right] \tag{7}$$

This model assumes a normal distribution of R_p, as has been found for other species when all pores per plate are measured (Jensen et al., 2012a). We also found the measured pore radii of our study species, Q. rubra, to be normally distributed. In the above equation, N is the total number of pores in a sieve plate (the adjusted pore number per sieve area as discussed in the *Image Analysis* section multiplied by the number of sieve areas); $\alpha = \frac{8l_p}{3\pi\bar{r}_p}$ and $\beta = \frac{\sigma}{\bar{r}_p}$ where $\bar{r}_p$ is the average pore radius and σ is the standard deviation. Finally, summing the resistance of the sieve element lumen with the resistance of one sieve plate results in the equation for the total hydraulic resistance of a sieve element:

$$R_{total} = \frac{8\eta L_{se}}{\pi r_{se}^4} + \frac{3\eta}{r_p^3} \frac{1}{N} \left[\frac{1}{1+3\beta^2} + \frac{\alpha}{1+6\beta^2+3\beta^4} \right] \tag{8}$$

While R_{total} provides an aggregate measure of how phloem anatomy across different size classes and sampling heights impacts sieve element hydraulic resistance, it is a biased estimate of transport efficiency. This is because phloem sap in a tree with shorter sieve elements must pass through sieve plate pores more frequently than in a tree with longer sieve element lumens. Therefore, to enable unbiased comparison of transport efficiency across different classes and sampling positions, we calculated a standardized measure of total resistance for each class and sampling position by multiplying R_{total} by the dimensionless factor *mean sieve element length/meter* (i.e., the number of sieve elements contained in a meter of transport distance).

Statistical analyses

We analyzed the effects of the factors individual tree identity, size (height) class, and sampling location on sieve element properties. All factors were treated as fixed, including tree identity. While a random sample of trees in each height class would have provided confidence intervals characterizing the population of all potentially chosen trees, as our choice of trees was constrained by access and availability to a relatively small number of trees, random sampling was not possible;

we therefore chose a fixed sample of three healthy trees in each size class. As not all sampling positions occur within each size class, we analyzed the effect of sampling position crossed with tree identity in separate ANOVAs for each size class. To compare anatomy across the different size classes at the "top" and "base" sampling positions (with the single sampling position of the smallest size class serving as both), we constructed ANOVAs with tree identity nested within size class. We chose a standard $\alpha = 0.05$ as the cut-off for significance in our ANOVAs and Tukey–Kramer honestly significant difference (HSD) to test for multiple post-hoc comparisons between sampling positions and size classes and to construct simultaneous 95% confidence intervals for the means. We also plotted the data for all size classes in terms of distance from the top, calculated as the difference between the mean tree height and mean sample height for each sampling location within a size class, and fit a power-law type of relationship (i.e., $y = ax^b$) between this distance and anatomy to generate allometric scaling exponents comparable to previous work (Petit and Crivellaro, 2014).

RESULTS

Sieve element length

Sieve element lumen length differed significantly as a function of sampling height only in the tallest size class of trees (21 m,

$F_{4, 135} = 3.47$, $p < 0.01$; 7 m, $F_{2, 81} = 2.8$, $p = 0.07$; 2 m, $F_{1, 54} = 0.037$, $p = 0.85$; Fig. 3A). In contrast to this weak sensitivity to position, sieve element lumen length exhibited a strong response to overall tree height, doubling from the smallest to largest size class ($F_{3, 326} = 68.7$, $p < 0.0001$; Fig. 3A). Plotting sieve element lumen length as a function of distance from the top showed that the data from all size classes did appear to collapse to a single power-law relationship (Fig. 3B). However, close inspection (and Fig. 3A) shows that this scaling relationship between distance from the top and sieve element length does not hold within groups of trees of the same size (or individual trees), but is entirely driven by the differences that exist between trees of different heights (i.e., a size class effect).

Sieve element radius

In contrast to length, sieve element radius differed significantly and importantly as a function of sampling height within the two tallest size classes (21 m, $F_{4, 135} = 85.47$, $p < 0.0001$; 7 m, $F_{2, 81} = 107.6$, $p < 0.0001$; Fig. 3C). For both of these size classes, the mean sieve element radius increased toward the base of the tree such that the mean radii at the base of the trees were approximately twice as large as the mean radii of the sieve elements at the top of the tree. However, in the largest size class, increases in sieve element radius appeared to saturate, such that the differences between the lowest three sampling positions (beneath the live crown) were both nonsignificant and small. The differences across size classes in mean sieve element radii at the basal position were both significant and important, varying from 8.4 μm in the smallest size class to 27.4 μm in the largest size class, even as the mean radius at the top of the tree did not differ significantly between the three larger size classes. Plotting the data as a function of distance from the top showed that sieve element radius may vary for all size classes as a single power-law function of distance from the plant apex (Fig. 3D). However, for the tallest size class, such a power-law fit is counter-indicated by the lack of significant changes in sieve element radius across the three most basal sampling positions.

Sieve plate pore radius

Broadly similar to the behavior of sieve element radius, sieve plate pore radius varied as a function of sampling height within size classes (21 m, $F_{4, 3330} = 821.5$, $p < 0.0001$; 7 m, $F_{2, 810} = 290.75$, $p < 0.0001$; 2 m, $F_{1, 606} = 215.8$, $p < 0.0001$). Mean sieve pore radius increased basipetally, exhibiting a saturating behavior with increasing distance from the apical region in the two larger size classes (Fig. 4A). Within size classes, the ratio of basal to apical radii varied from a factor of about two in the tallest (21 m), to 1.66 in the 7 m, and 1.35 in the 2 m size class: Due to the 3rd power dependence on pore radii of flow through
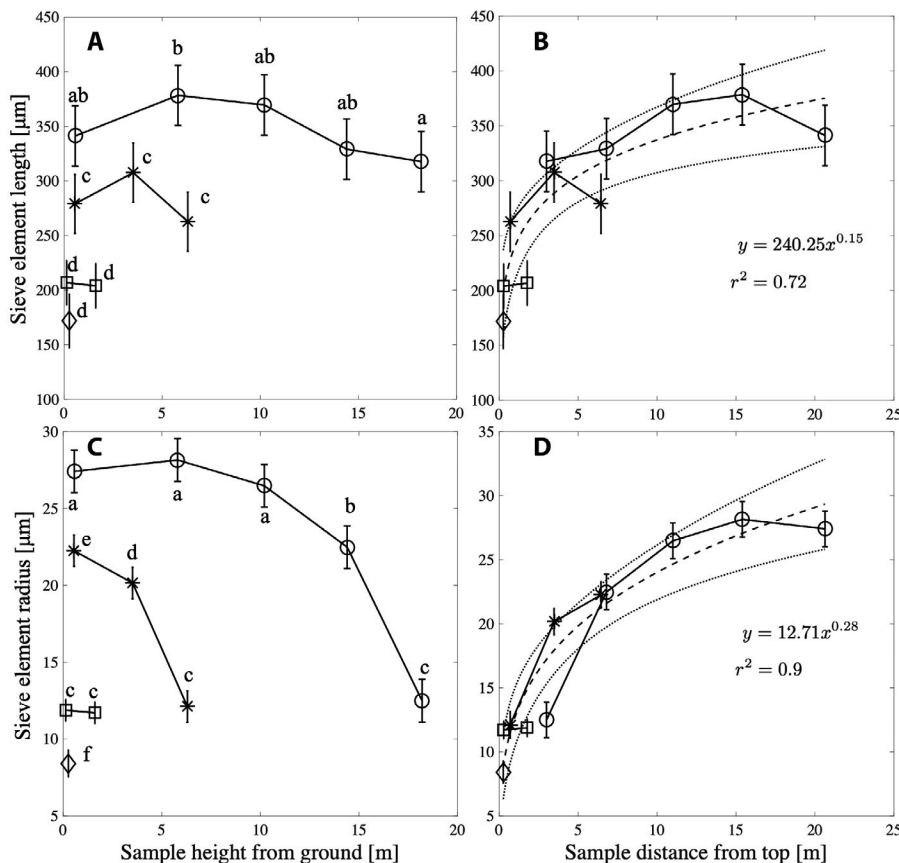

FIGURE 3. (A, B) Mean sieve element lumen length and (C, D) sieve element radius versus location on the stem, expressed as sampling height (A, C) or distance from the top (B, D) for each size class (diamonds, 0.5 m; squares, 1.9 m; asterisks, 7 m; circles, 21.2 m). Error bars represent 95% CIs; $n = 30$ for length, 90 for radius. Lower case letters denote significant differences based on Tukey–Kramer HSD, $\alpha = 0.05$.
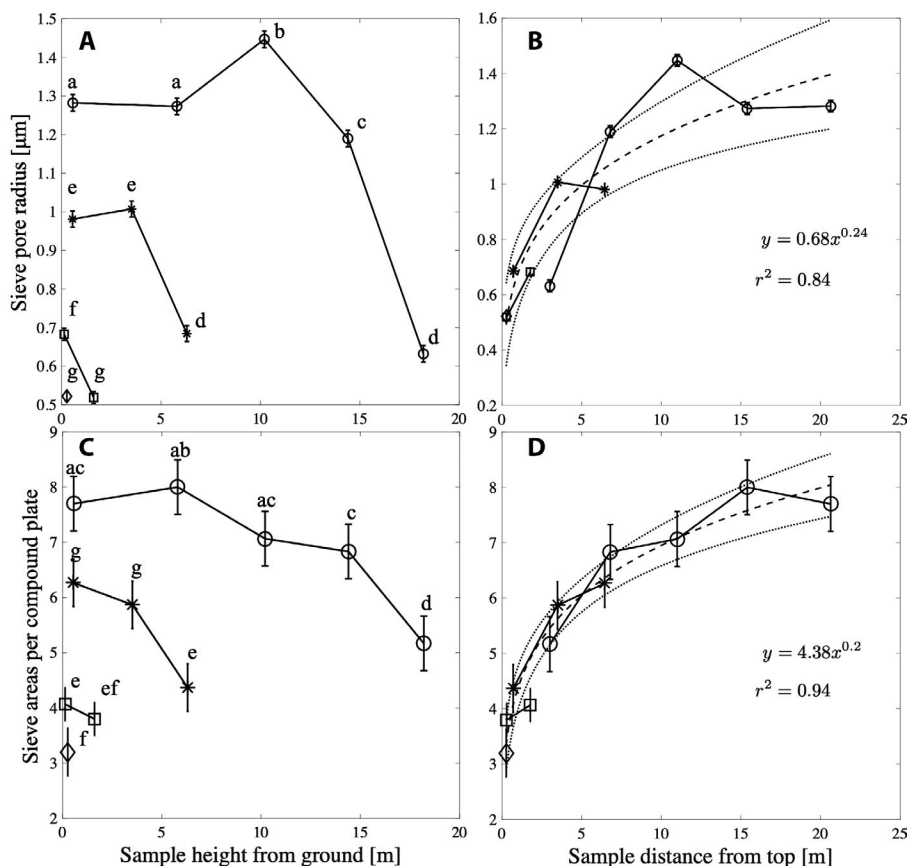
Equations in figure B: $y = 240.25x^{0.15}$, $r^2 = 0.72$

Equations in figure D: $y = 12.71x^{0.28}$, $r^2 = 0.9$

FIGURE 4. (A, B) Mean sieve pore radius and (C, D) mean number of sieve areas per compound plate versus location on the stem, expressed as sampling height (A, C) or distance from the top (B, D) for each size class (diamonds, 0.5 m; squares, 1.9 m; asterisks, 7 m; circles, 21.2 m). Error bars represent 95% CIs. For sieve plate pore radius, at each sampling position, $n = 456$ for the 0.5 m size class, 306 for 1.9 m, 273 for 7 m, and 669 for 21.2 m; for number of sieve areas, $n = 30$. Lower case letters denote significant differences based on Tukey–Kramer HSD, $a = 0.05$).

plates (Eq. 7), increasing the radius by a factor of 1.35 will reduce the hydraulic resistance to less than half (~0.4) of its initial value. Across size classes, sieve pore radii varied significantly at both the apical and basal positions (apical, $F_{3, 1812} = 161.4$, $p < 0.0001$; basal, $F_{3, 1080} = 780$, $p < 0.0001$). The overall pattern was closer to that exhibited by sieve element radius than sieve element length, with a power-law fit based on distance from the top again capturing much of the variation in radius across and within all size classes (Fig. 4B), and again despite apparent saturation in the largest size class.

Number of sieve areas per compound sieve plate

The number of sieve areas per compound plate ranged from 2 to 10 sieve areas per plate, increasing basipetally in a manner similar to that of both pore and sieve element radius (21 m, $F_{4, 135} = 19.45$, $p < 0.0001$; 7 m, $F_{2, 81} = 21.4$, $p < 0.0001$; Fig. 4C). For both the 7 m and 21 m size classes, the number of sieve areas per plate increased significantly between the crown and stem; however, for the 2 m size class, the number of sieve areas per plate showed a similar but nonsignificant difference between the two (apical and basal) sampling positions. A comparison of the number of sieve areas per compound plate at the basal and apical sampling heights across all of the size classes demonstrated a significant effect of plant size at both sampling locations (basal,

$F_{3, 108} = 84$, $p < 0.0001$; apical, $F_{3, 108} = 20.6$, $p < 0.0001$). Post hoc analyses showed that, for the basal measurements, the number of sieve plates per compound plate increased significantly, varying by a factor of 2 with increasing plant size across the three larger size classes. In contrast, the number of sieve areas per plate at the top of the trees was more consistent among size classes; though the difference between the 21 m and 7 m size classes was significant, the magnitude of the difference was small relative to the differences between basal positions. As a result, variation in sieve area number is well captured by a single relationship with distance from the top across all size classes (Fig. 4D), despite nonsignificant differences between the three lowest sampling locations in the largest size class (Fig. 4C).

Sieve plate angle and pore density

Sieve plate angle did not show significant trends as a function of height within size classes (Fig. 5A). In the tallest class, the effect of sampling height was significant ($F_{4, 135} = 4.97$, $p < 0.001$), but contrary to our expectations for this variable, the sieve plate angle was *less* steep at the base of the largest trees. We had expected a *steeper* plate angle as, other things being equal, plate area (and so conductance) increases as sieve element radius squared, while lumen conductance increases as sieve element radius to the fourth power, and a steeper angle would introduce further increases in plate surface area that could help to increase sieve pore area and keep plate and lumen conductance in balance. However, the differences in the mean plate angle were small: approximately 59° at the base of the largest trees compared to approximately 67° at the higher sampling heights. Furthermore, there was considerable variation in sieve plate angle at each sampling height, which may reflect the difficulty in measuring sieve plate angle accurately from tangential phloem sections due to variability in the positioning of the sieve plates. Across basal positions, there were no significant or important differences between the three larger size classes, with the mean sieve plate angle at the base of each size class only differing by ~9°. When plotted as a function of distance from the top, there was a trend in mean plate angle across size classes in a physiologically sensible direction—steeper in larger trees—but the only statistically significant post hoc result was that plate angles were less steep in the smallest compared to the three larger size classes (Fig. 5B). Pore number per sieve area showed no significant trends either within, or across, size classes (Fig. 5C, D).

Total hydraulic resistance of sieve elements

The total calculated resistance (mPa s μm^{-3}) to flow through an average sieve element at each sampling location in each tree (Fig. 6A, B) showed that, in the 7 m and 21 m classes, total resistance decreased by an order of magnitude from the apical to the
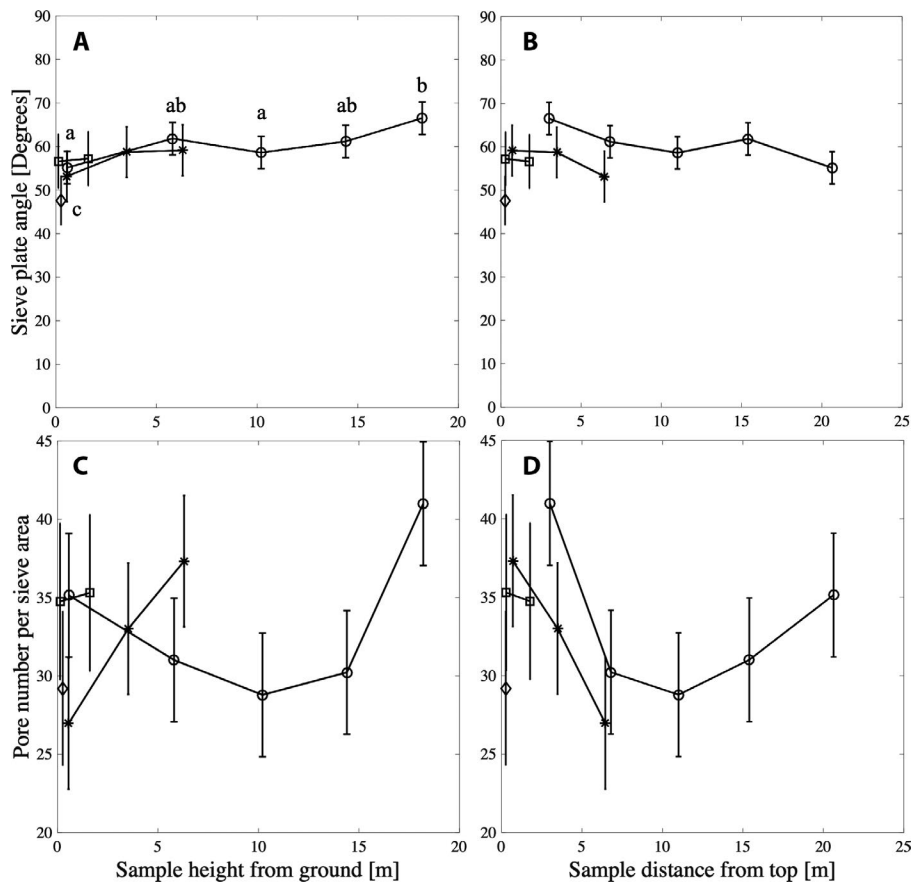
FIGURE 5. (A, B) Mean sieve plate angle and (C, D) mean pore number per sieve area versus location on the stem, expressed as sampling height (A, C) or distance from the top (B, D) for each size class (diamonds, 0.5 m; squares, 1.9 m; asterisks, 7 m; circles, 21.2 m). Error bars represent 95% CIs; *n* = 10. Lower case letters denote significant differences based on Tukey–Kramer HSD, *α* = 0.05.

is consistent with previous work (Savage et al., 2017), though it is in contrast to the typical proportions for xylem elements, which have been found to be closer to the expected (co-limiting) division of 50% end wall versus 50% lumen resistance. Yet, due to the persistence at maturity of a layer of endoplasmic reticulum, plastids, and mitochondria lining the sieve element wall (Evert, 2006), wall-to-wall measurements of sieve element diameter may overestimate the effective diameter with respect to mass flow; it has been suggested that accounting for this effect produces more equal divisions of total sieve element resistance between sieve plate and lumen (Jensen et al., 2012a). Nevertheless, we expect the trends reported here in sieve element radius to be robust, as it seems doubtful that variation in the thickness of wall bound organelles and membrane systems could approach the range of variation (8–27 μm) for sieve element radii in our data (Fig. 3C,D). Finally, both the hydraulic resistances of the sieve element lumen and sieve element plates show similar responses to distance from the apex as their radii terms (Fig. 7), reflecting the importance of the sieve element radius term in the calculation of lumen resistance and the sieve plate pore radius in the calculation of plate resistance.

"Whole-plant" hydraulic resistance

To gain insight into whether the increases in sieve plate pore radius and sieve element length and radius are sufficiently large that the "whole-plant" hydraulic resistance of the phloem might be independent of tree size, we integrated the total resistance of a file of sieve elements along the individual heights of each tree, based on the total sieve element resistivity at each sampling height (Fig. 6): the resistance over the distances between sampling heights was estimated by averaging the resistances of the bounding sampling heights. The resulting mean "whole-plant" resistances across each class, while highly variable, showed no trend across height class (Fig. 8). It should be noted that this estimate represents the resistance of a single sieve tube spanning the height of the whole tree, and not the true "whole-plant" total resistance of the entire phloem; we could not estimate the latter as we did not have a reliable way to quantify the number of sieve element cells in phloem tissue cross sections.

Although the within-size class estimates are highly variable, the tree with the lowest resistance, found in the smallest size class, achieved that extreme value due to an unusually high mean density of pores per unit sieve area, 52, versus the mean across all size classes and sampling positions of 32. Yet, pore density was not a variable that showed a systematic response to either location or tree size, with the implication it may be less plastic and more stochastic along a stem. In addition, given that the whole plant resistances of the 0.5 m size class are based on a single sampling height, estimates
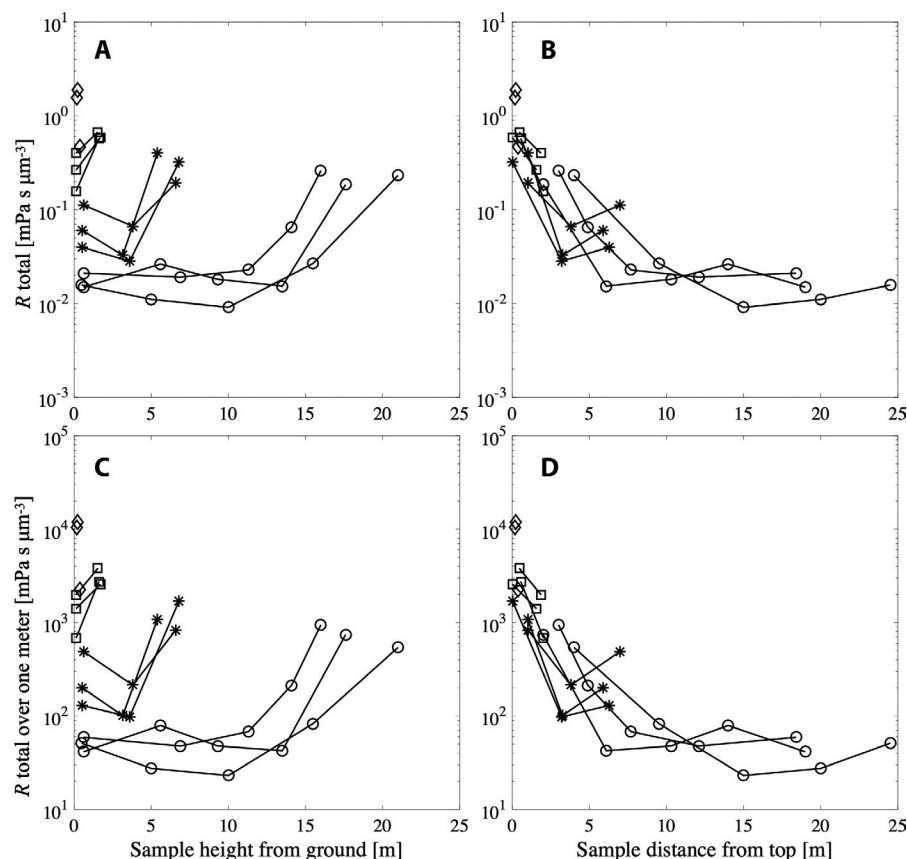
basal sampling height. The total resistance of the sieve elements at the top of the tree tended to decrease with increasing tree size, while the total resistance at the base of the trees decreased approximately 50-fold across increasing tree size classes. The pattern of variation observed in many (but not all) of the component variables (sieve element radius, pore radius, and sieve area number) was therefore conserved in total sieve element resistance, a result likely driven by the importance of the radii terms in the calculation of hydraulic resistance (Eq. 6). Like these variables, total resistance in the 21 m class appeared to reach a constant value at the three lower sampling positions. Incorporating the effect of differences in sieve element length by calculating the total resistance normalized to a 1 m length (mPa s μm⁻³; hence a kind of "total resistivity") preserved this response as well, despite near constant sieve element length along the stem within a size class (Fig. 6C, D).

Contributions of the sieve element lumen and sieve element plate to hydraulic resistance

Total hydraulic resistance by convention represents the sum of the resistance contributed by the sieve element lumen (Fig. 7A, B) and the resistance contributed by one sieve plate (Fig. 7C, D). On average, 82% of the total resistance was due to the sieve plates: for 21 m, 79%; 7 m, 83%; 2 m, 87%; 0.5 m, 86%. Such a strong dominance of plate resistance

FIGURE 6. (A, B) Total hydraulic resistance *R* of individual sieve elements and (C, D) total hydraulic resistance of a file of sieve elements calculated for a standard length of 1 m plotted versus sampling height from the ground (A, C) and versus distance from the top of tree (B, D) for each size class (diamonds, 0.5 m; squares, 1.9 m; asterisks, 7 m; circles, 21.2 m).

for this size class were more sensitive than the larger classes to noise in the pore number data. Nevertheless, assuming a conserved flow rate and sap viscosity across trees of different size, and neglecting radial in/out flow, these results point to the possibility of a "whole-plant" axial pressure drop in the phloem independent of tree height.

DISCUSSION

The combination of large modeled resistances in phloem sieve tubes with small measured pressures in the leaves has long presented an apparent paradox as to how carbohydrates are transported in trees (Thompson and Holbrook, 2003; Gould et al., 2005; Thompson, 2006; Hölttä et al., 2009; Jensen et al., 2009; Knoblauch and Peters, 2010; Mencuccini et al., 2011). In response to this well-established puzzle, however, a seemingly simple answer is emerging: the size and structure of the phloem cells varies along the length of the transport pathway, decreasing the hydraulic resistance such that carbohydrate transport appears unproblematic even under the low pressures generated by passive-loading species (Knoblauch et al., 2016; Savage et al., 2017). Here we have attempted to characterize the patterns of anatomical variation occurring along the stem of different ontogenetic stages of a single species.

In the studies that have reported changes in sieve element dimensions and sieve plate structure with tree height across species

(Petit and Crivellaro, 2014; Liesche et al., 2017; Savage et al., 2017), either the phylogenetic breadth or intensity of individual sampling precluded intensive sampling of multiple individuals of different sizes. For the red oak data presented here, aggregating the data from all 12 trees shows that variations from apex to base in sieve element length, sieve element radius, sieve plate pore radius, sieve area number are well described by a power law with exponents (0.15–0.28) broadly consistent with those previously reported for phloem anatomical characteristics (0.14–0.4: Petit and Crivellaro (2014); ~0.3: Savage et al. (2017)). However, our sampling shows that the apparent trend of sieve element length with distance from the top seen for data aggregated across all size classes is due to a height class effect; variation along the stems of individual trees makes no contribution. These results, taken together, demonstrate that height-related trends in phloem transport capacity are influenced by (at least) two different metrics: distance from the plant apex and tree size.

A response of phloem development to two metrics would also help explain the apparent pattern of near constant sieve element radius, sieve plate pore radius, and sieve area number in the stem below the live crown, as observed in the largest size class: if this "saturated" value did not change with height class (i.e., in a manner similar to sieve element length), the total resistance of a single sieve tube running from apex to base would increase with increasing plant height, contrary to our data. More intensive sampling of the 7 m size class is required to resolve whether their sieve tube anatomy approaches constant values down the stem or if the anatomy of all size classes simply follows the same distance from top relationship. It is important to note, however, that a developmental response only to distance from the top would not be sufficient to prevent increases in total sieve tube resistance with increases in tree height: even if the response to height does not saturate below the live crown (e.g., sieve element radius increases continually with distance from the top), each increment of height will add a small but finite amount of resistance. Indeed, for pipe flow, it is readily seen that the radius of the entire pipe (not just marginal increases) must grow as length raised to the ¼ power for hydraulic resistance to be entirely independent of length (Eq. 2).

Some support for the idea that phloem anatomy could reach a fixed state below the live crown can be found in previous work: the intensive sampling of Petit and Crivellaro (2014) shows that for a 6-m willow (*Salix eleagnos*), there was no trend in the hydraulic diameter of the sieve elements from 3 to 6 m below the apex, a pattern mirrored by vessel hydraulic diameter, although ash (*Fraxinus excelsior*) showed more continuous increases. The general concept of transport capacity changing at a transition from a source to a translocation region has also been demonstrated in the veins of
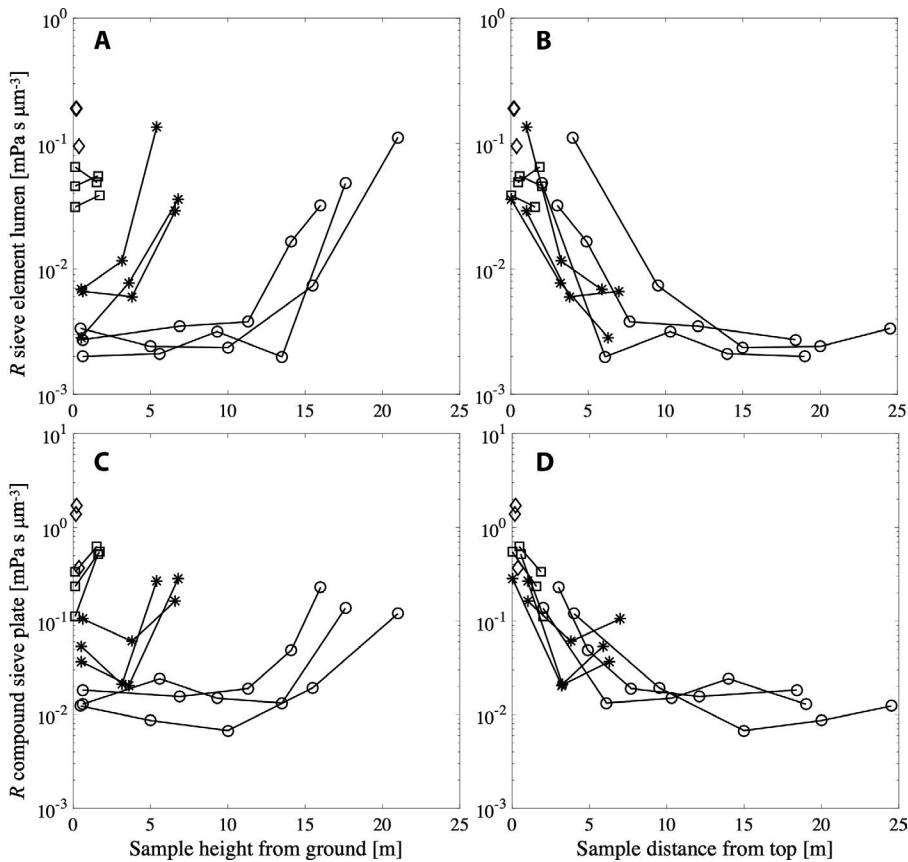
FIGURE 7. (A, B) Hydraulic resistance *R* of the sieve element lumen and (C, D) compound sieve plate plotted versus sampling height from the ground (A, C) and versus distance from the top of tree (B, D) for each size class (diamonds, 0.5 m; squares, 1.9 m; asterisks, 7 m; circles, 21.2 m).
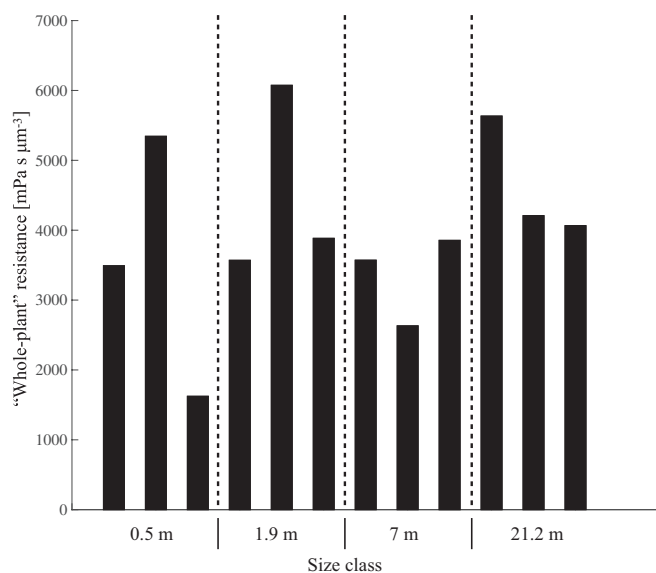

FIGURE 8. Mean "whole-plant" resistance, defined as the total hydraulic resistance (R_{total}) of a file of sieve elements integrated piecewise over the individual tree heights in each size class.

Populus leaves by Carvalho et al. (2017a), where the total conductive area in the phloem was found to decrease linearly from the 4th to 7th vein orders (source region) before saturating for the 0th to 3rd vein orders (translocation region). Importantly, Carvalho et al. (2017a) obtained this result from a measure of total conductive area (measurements of conductive area in individual veins yielded a reversed pattern). While this cross-sectional analysis can be accomplished in the leaves (c.f. Carvalho et al., 2017b), we did not attempt this allometric analysis because of the difficulty of identifying all phloem sieve elements in cross section in the (living) trunk. We also note that the analogy between leaf and whole-tree networks is imperfect. Our samples within the live crown would not be expected to contain actual loading zones, as occur in the finest leaf veins; nevertheless, the live crown could still be considered a region of converging flows that might impose different constraints on anatomy than the flow in the unbranched main stem.

Asymptotes, or convergence on a fixed value, have also been reported in xylem allometry. Bettiati et al. (2012) found that in *Picea abies*, total conducting area and tracheid hydraulic diameter followed a power-law relationship with distance from the apex within the live crown, but then remained constant or demonstrated slight declines respectively down the stem. Williams et al. (2019) report that in tall trees (*Sequoia sempervirens*, *Sequoiadendron giganteum*, *Eucalyptus regnans*) xylem conduit diameters began to deviate from a power-law relationship with distance from the top about half way down the stems, approaching a fixed value toward the base.

Such reports together with this study suggest the potential importance of the live crown to stem transition in comparative studies of xylem and phloem hydraulic architecture, as well as the utility of a focus on integrated responses to both distance from the shoot apex and overall plant size. Although many studies of xylem anatomy report a general trend of basipetal vessel widening with tree height (Anfodillo et al., 2006; Petit et al., 2010; Olson et al., 2014; Petit and Crivellaro, 2014; Jyske and Hölttä, 2015; Jacobsen et al., 2018), the response of xylem conduits to the combination of both distance from the top and overall tree size or ontogenetic stage has yet to be fully explored. Further investigation distinguishing the effects on vascular architecture of these two height-related metrics could provide new information on the mechanistic basis of xylem and phloem allometric scaling and hydraulic optimization.

CONCLUSIONS

This study presents a new perspective on phloem hydraulic resistance in trees by demonstrating that variations in phloem anatomy

at different heights do not necessarily vary with distance from the plant apex in a simple manner within individual plants. Rather, sieve cell allometry responds both to position and to some measure of total plant size (e.g., height, live crown volume). Our data also point toward the possibility that the total resistance of a continuous file of sieve elements spanning the length of the above ground portion of red oak trees may not increase from saplings to canopy trees, which would not strictly be expected if trees of different sizes or ontogenetic stages followed a single distance from the top scaling relationship: some sensitivity to overall tree size is required. Further investigation of these variations in conduit resistance in the context of ontogeny could provide insights into the developmental mechanisms controlling these patterns, as well as the allometric relationships useful for scaling individual plant physiological responses to forest level dynamics.

ACKNOWLEDGMENTS

AUTHOR CONTRIBUTIONS

N.M.H., J.A.S., and L.E.C. conceived the study. L.E.C. performed the fieldwork, sample preparation, and microscopy. L.E.C., J.A.S., and F.E.R. analyzed the data. L.E.C., F.E.R., and N.M.H. wrote the manuscript.

DATA AVAILABILITY

All data are available at the Harvard Forest Data Archive (https://harvardforest.fas.harvard.edu/harvard-forest-data-archive).

LITERATURE CITED

Aloni, R. 2015. Ecophysiological implications of vascular differentiation and plant evolution. *Trees* 29: 1–16.

Anfodillo, T., V. Carraro, M. Carrer, C. Fior, and S. Rossi. 2006. Convergent tapering of xylem conduits in different woody species. *New Phytologist* 169: 279–290.

Bettiati, D., G. Petit, and T. Anfodillo. 2012. Testing the equi-resistance principle of the xylem transport system in a small ash tree: empirical support from anatomical analyses. *Tree Physiology* 32: 171–177.

Canny, M. J. 1973. Phloem translocation. Cambridge University Press, Cambridge, UK.

Carvalho, M. R., R. Turgeon, T. Owens, and K. J. Niklas. 2017a. The scaling of the hydraulic architecture in poplar leaves. *New Phytologist* 214: 145–157.

Carvalho, M. R., R. Turgeon, T. Owens, and K. J. Niklas. 2017b. The hydraulic architecture of ginkgo leaves. *American Journal of Botany* 104: 1285–1298.

Dengler, N. G. 2001. Regulation of vascular development. *Journal of Plant Growth Regulation* 20: 1–13.

Esau, K., and V. I. Cheadle. 1961. An evaluation of studies on ultrastructure of sieve plates. *Proceedings of the National Academy of Sciences, USA* 47: 1716–1726.

Evert, R. F. 2006. Esau's plant anatomy meristems, cells, and tissues of the plant body: their structure, function, and development. John Wiley, Hoboken, NJ, USA.

Gould, N., M. R. Thorpe, O. Koroleva, and P. E. H. Minchin. 2005. Phloem hydrostatic pressure relates to solute loading rate: a direct test of the Münch hypothesis. *Functional Plant Biology* 32: 1019–1026.

Hölttä, T., M. Mencuccini, and E. Nikinmaa. 2009. Linking phloem function to structure: analysis with a coupled xylem–phloem transport model. *Journal of Theoretical Biology* 259: 325–337.

Jacobsen, A. L., J. Valdovinos-Ayala, F. D. Rodriguez-Zaccaro, M. A. Hill-Crim, M. I. Percolla, and M. D. Venturas. 2018. Intra-organismal variation in the structure of plant vascular transport tissues in poplar trees. *Trees* 32: 1335–1346.

Jensen, K. H., K. Berg-Sørensen, H. Bruus, N. M. Holbrook, J. Liesche, A. Schulz, M. A. Zwieniecki, and T. Bohr. 2016. Sap flow and sugar transport in plants. *Reviews of Modern Physics* 88: 035007.

Jensen, K. H., K. Berg-Sørensen, S. M. M. Friis, and T. Bohr. 2012b. Analytic solutions and universal properties of sugar loading models in Münch phloem flow. *Journal of Theoretical Biology* 204: 286–296.

Jensen, K. H., D. L. Mullendore, N. M. Holbrook, T. Bohr, M. Knoblauch, and H. Bruus. 2012a. Modeling the hydrodynamics of phloem sieve plates. *Frontiers in Plant Science* 3: 151.

Jensen, K. H., E. Rio, R. Hansen, C. Clanet, and T. Bohr. 2009. Osmotically driven pipe flows and their relation to sugar transport in plants. *Journal of Fluid Mechanics* 636: 371–396.

Jensen, K. H., J. A. Savage, and N. M. Holbrook. 2013. Optimal concentration for sugar transport in plants. *Journal of the Royal Society Interface* 10: 20130055.

Jyske, T., and T. Hölttä. 2015. Comparison of phloem and xylem hydraulic architecture in *Picea abies* stems. *New Phytologist* 205: 102–115.

Knoblauch, M., and W. S. Peters. 2010. Münch, morphology, microfluidics – our structural problem with the phloem. *Plant, Cell & Environment* 33: 1439–1452.

Knoblauch, M., J. Knoblauch, D. L. Mullendore, J. A. Savage, B. A. Babst, S. D. Beecher, A. C. Dodgen, et al. 2016. Testing the Münch hypothesis of long distance phloem transport in plants. *Elife* 5: e15341.

Lang, A. 1979. A relay mechanism for phloem translocation. *Annals of Botany* 44: 141–145.

Liesche, J., M. R. Pace, Q. Xu, Y. Li, and S. Chen. 2017. Height-related scaling of phloem anatomy and the evolution of sieve element end wall types in woody plants. *New Phytologist* 214: 245–256.

Losada, J. M., and N. M. Holbrook. 2019. Scaling of phloem resistance in stems and leaves of the understory angiosperm shrub *Illicium parviflorum*. *American Journal of Botany* 106: 244–259.

Mäkelä, A., L. Grönlund, P. Schiestl-Aalto, T. Kalliokoski, and T. Hölttä. 2019. Current-year shoot hydraulic structure in two boreal conifers—implications of growth habit on water potential. *Tree Physiology* 39: 1995–2007.

McCulloh, K. A., J. S. Sperry, and F. R. Adler. 2003. Water transport in plants obeys Murray's law. *Nature* 421: 939–942.

Mencuccini, M., T. Hölttä, and J. Martínez-Vilalta 2011. Comparative criteria for models of the vascular transport systems of tall trees. *In* F. C. Meinzer, B. Lachenbruch, and T. E. Dawson [eds.], Size- and age-related changes in tree structure and function, vol. 4, Tree physiology, 303–339. Dordrecht, Netherlands, Springer.

Mullendore, D. L., C. W. Windt, H. Van As, and M. Knoblauch. 2010. Sieve tube geometry in relation to phloem flow. *Plant Cell* 22: 579–593.

Münch, E. 1930. Die Stoffbewegungen in Der Pflanze. Fischer, Jena, Germany.

Murray, C. D. 1926. The physiological principle of minimum work. I. The vascular system and the cost of blood volume. *Proceedings of the National Academy of Sciences, USA* 12: 207–214.

Olson, M. E., T. Anfodillo, J. A. Rosell, G. Petit, A. Crivellaro, S. Isnard, C. Leon-Gomez, et al. 2014. Universal hydraulics of the flowering plants: Vessel diameter scales with stem length across angiosperm lineages, habits and climates. *Ecology Letters* 17: 988–997.

Petit, G., and A. Crivellaro. 2014. Comparative axial widening of phloem and xylem conduits in small woody plants. *Trees* 28: 915–921.

Petit, G., S. Pfautsch, T. Anfodillo, and M. A. Adams. 2010. The challenge of tree height in *Eucalyptus regnans*: when xylem tapering overcomes hydraulic resistance. *New Phytologist* 187: 1146–1153.

Phillips, R. J., and S. R. Dungan. 1993. Asymptotic analysis of flow in sieve tube walls with semipermeable walls. *Journal of Theoretical Biology* 162: 465–485.

Savage, J. A., S. D. Beecher, L. Clerx, J. T. Gersony, J. Knoblauch, J. M. Losada, K. H. Jensen, et al. 2017. Maintenance of carbohydrate transport in tall trees. *Nature Plants* 3: 965–972.

Sevanto, S. 2014. Phloem transport and drought. *Journal of Experimental Botany* 65: 1751–1759.

Taiz, L., E. Zeiger, I. M. Moller, and A. Murphy. 2015. Plant physiology and development, 6th ed. Sinauer, Sunderland, MA, USA.

Thompson, M. V. 2006. Phloem: the long and the short of it. *Trends in Plant Science* 11: 26–32.

Thompson, M. V., and N. M. Holbrook. 2003. Application of a single-solute non-steady-state phloem model to the study of long-distance assimilate transport. *Journal of Theoretical Biology* 220: 419–455.

Turgeon, R. 2010. The puzzle of phloem pressure. *Plant Physiology* 154: 578–581.

Tyree, M. T., A. L. Christy, and J. M. Ferrier. 1974. A simpler iterative steady state solution of Münch pressure-flow systems applied to long and short translocation paths. *Plant Physiology* 54: 589–600.

West, G. B., J. H. Brown, and B. J. Enquist. 1999. A general model for the structure and allometry of plant vascular systems. *Nature* 400: 664–667.

Williams, C. B., T. Anfodillo, A. Crivellaro, M. Lazzarin, T. E. Dawson, and G. W. Koch. 2019. Axial variation of xylem conduits in the Earth's tallest trees. *Trees* 33: 1299–1311.